Behavior of excited argon atoms in inductively driven plasmas

G. A. Hebner and P. A. Miller

Sandia National Laboratories

Albuquerque NM 87185-1423

Abstract

Laser induced fluorescence has been used to measure the spatial distribution of the two lowest energy argon excited states, $1s_5$ and $1s_4$, in inductively driven plasmas containing argon, chlorine and boron trichloride. The behavior of the two energy levels with plasma conditions was significantly different, probably because the $1s_5$ level is metastable and the $1s_4$ level is radiatively coupled to the ground state but is radiation trapped. The argon data is compared with a global model to identify the relative importance of processes such as electron collisional mixing and radiation trapping. The trends in the data suggest that both processes play a major role in determining the excited state density. At lower rf power and pressure, excited state spatial distributions in pure argon were peaked in the center of the discharge, with an approximately Gaussian profile. However, for the highest rf powers and pressures investigated, the spatial distributions tended to flatten in the center of the discharge while the density at the edge of the discharge was unaffected. The spatially resolved excited state density measurements were combined with previous line integrated measurements in the same discharge geometry to derive spatially resolved, absolute densities of the $1s_5$ and $1s_4$ argon excited states and gas temperature spatial distributions. Fluorescence lifetime was a strong function of the rf power,

DISCLAIMER

DISCLAIMER

Portions of this document may be illegible in electronic image products. Images are produced from the best available original document.

pressure, argon fraction and spatial location. Increasing the power or pressure resulted in a factor of two decrease in the fluorescence lifetime while adding Cl_2 or BCl_3 increased the fluorescence lifetime. Excited state quenching rates are derived from the data. When Cl_2 or BCl_3 was added to the plasma, the maximum argon metastable density depended on the gas and ratio. When chlorine was added to the argon plasma, the spatial density profiles were independent of chlorine fraction. While it is energetically possible for argon excited states to dissociate some of the molecular species present in this discharge, it does not appear to be a significant source of dissociation. The major source of interaction between the argon and the molecular species BCl_3 and Cl_2 appears to be through modification of the electron density.

I. Introduction

High electron density inductively coupled plasma (ICP) systems are finding increasing applications in the areas of microelectronic processing, cleaning and illumination. In order to understand the fundamental plasma physics mechanisms and to provide data to benchmark codes, many experiments have focused on inductive discharges in argon. Compared with molecular gases, argon has the advantage of a relatively complete set of cross sections and a minimum number of gas phase species. However, many applications add one or more other gases, depending on the process requirements. For example, Cl_2 and BCl_3 containing plasmas are used for microelectronic interconnect metal definition and III – V material etching.[1,2,3] In addition, argon is commonly added to some discharges as an actinometry standard.[4] As a result, there is interest in investigating both pure argon discharges and mixtures of argon with molecular gases.

The lowest-energy excited states of argon often have populations that are comparable to the electron density, a few 10^{11} cm^{-3}.[5] The $1s_5$ and $1s_3$ energy levels (Paschen notation) are metastable while the $1s_4$ and $1s_2$ levels are radiatively coupled to the ground state but are radiation trapped. Under some discharge conditions, these energy levels can serve as a reservoir of species that have enough energy ($\approx$ 11.5 eV)to contribute in principle to ionization, excitation or molecular dissociation. A number of measurements using different techniques have been reported to characterize these excited states. Miller et al have used optical self absorption to measure the relative, line-integrated density of several argon and chlorine excited states.[6] The technique provides a relatively simple way to monitor excited state densities. However, absolute density calibration can be difficult due to unknown emission and absorption lineshapes.

McMillan et al used laser induced fluorescence (LIF) to measure the spatially resolved relative metastable density in a parallel plate discharge.[7] They noted enhanced metastable densities at the edge of the electrodes, presumably due to the enhanced electric fields at the electrode edges. Scheller et. al measured the density of the $1s_5$ metastable level in gas mixtures containing SF_6, Cl_2 and BCl_3 in a parallel plate discharge geometry and proposed a model to explain some of the observed phenomena.[8] Based upon their observations, they proposed that argon metastables only indirectly influence molecular dissociation by modifying the ion density via Penning reactions. Leonhardt et al examined the metastable $1s_5$ and $1s_3$ levels and the radiatively coupled $1s_4$ level in an ECR discharge system containing Ar / Cl_2 gas mixtures using diode laser absorption.[9] They measured argon $1s_5$, $1s_4$ and $1s_3$ excited state densities that were 2 to 3 orders of magnitude less than the electron and ion density and concluded that metastables do not play a major role in the ionization balance. This is in contrast to our recent measurements in ICP systems where the metastable density was comparable to the electron density ($10^{11} - 10^{12}$ cm^{-3}).[5] Thus the role of argon metastables in ICP discharges containing Cl_2 or BCl_3 , is still unclear.

Since the argon $1s_5$, $1s_4$, $1s_3$ and $1s_2$ energy levels are within 0.28 eV of each other, electron collisional mixing between the levels can be an important population transfer process. For example, a significant loss process for the metastable levels is the collisional transfer from the metastable level to the $1s_4$ and $1s_2$ levels followed by subsequent loss via radiative transitions to the ground state.[8,10,11] Due to production by electron collisional transfer from the metastable levels and radiation trapping, the density of the $1s_4$ level can become comparable to the density of the $1s_5$ metastable level. Thus, this work includes both the $1s_5$ and $1s_4$ energy levels.

The goals of this work were to investigate the interaction of argon metastables and excited states with molecular gases and to provide data to validate codes developed recently for

high electron density plasmas. There are many examples of low pressure ICP models in gases containing a single species like argon or helium, or reactive gases such as Cl_2.[12,13,14,15] In general, those models capture the main trends observed in numerous experimental measurements. In contrast, models of gas mixtures are less well developed, due in part to the numerous and unknown interactions between the many molecular and atomic species that can be present. Several laboratories have reported recently the results from experiments in mixture of argon and other gases, but with different discharge geometries and excitation methods.[7,8,9] Our measurements complement and extend those results and advance several hypotheses concerning the complex features observed in some gas mixtures in inductively driven discharges. A more fundamental overall understanding of discharges in those gas mixtures would be advanced most rapidly by comparison of *all* the experimental results to a comprehensive model.

To establish an experimental baseline for comparison, this work will first examine the density trends in pure argon, followed by mixtures containing Ar, Cl_2 and BCl_3. This study is an extension of previous line integrated absorption and LIF measurements of the argon excited states using a single mode, cw laser to map the absorption lineshapes.[5] In that work, absorption spectroscopy was utilized to measure the spatially resolved density and temperature of the argon $1s_5$, $1s_4$, $1s_3$ and $1s_2$ (Paschen notation) energy levels and spatially resolved LIF was used to confirm the argon neutral temperatures and measure the metastable argon ion temperature. In the case of the absorption measurements, the analysis of the lineshape was clouded by a lack of information about the spatial distribution. In the present work, LIF was used to measure the spatial distribution of the $1s_5$ and $1s_4$ energy levels. By combining the results of the previous absorption measurements with the current spatially resolved density measurements, the absolute density of the spatially resolved excited state distributions can be derived and trends in the

neutral temperature distribution can be examined. The influence of Cl_2 and BCl_3 addition on the density of the $1s_5$ and $1s_4$ levels is also examined and correlated with previous measurements of Cl, BCl, Cl^+, Cl^-, and electron density.[16,17,18,19,20,21,22] In addition, excited state (3p state) quenching rates can be inferred from the fluorescence lifetime of the LIF. Finally, in an attempt to understand better the relative importance of competing processes in the argon discharges, we developed a simple global model for creation and destruction of all four 1s states. The model focused on the distinct behavior of the four closely coupled $1s_x$ levels and it did not include a plasma model.

II. Experimental configuration

The experiments were performed in a Gaseous Electronics Conference (GEC) rf reference reactor that has been modified to include an inductively coupled plasma source. Design and construction details of this system have been discussed previously.[23,24] Briefly, the induction coil was a five turn, 11 cm diameter, planar coil constructed from 1/8 inch diameter copper tubing. A 1-cm thick fused silica window separated the coil from the plasma. Distance from the window to the lower electrode was 3.8 cm. For these experiments, the lower electrode was grounded, and covered with a 15 cm diameter, bare, unpatterned, silicon wafer. Due to the design of the reactor, the clear view between the ICP source and the lower electrode was approximately 13 cm in the radial direction and 3.1 cm in the axial direction. Both the induction coil and the lower electrode were water cooled. Operation frequency was 13.56 MHz. In this work, the reported rf power was the forward power minus the reflected power at the input to the matching network. Previous work in this system has shown that for typical operating conditions, approximately 80 percent of the input power was deposited into the plasma.[5] For this

experiment, the discharge chamber and associated hardware were mounted on a two dimensional translation stage to facilitate spatial LIF measurements without translating the optics.

The laser and optical system used for this study was similar to previous LIF measurements in this discharge chamber.[15,16,18] For this work, a Nd:YAG pumped dye laser was frequency mixed to generate 395 and 404 nm radiation to excite the $1s_5$ to $3p_3$ and $1s_4$ to $3p_3$ transitions, respectively. The laser pulse width was approximately 8 ns, and the energy was attenuated to 0.5 mJ per pulse. The laser was unfocused, with a beam diameter of approximately 6 mm. Fluorescence from the $3p_3$–to-$1s_2$ transition at 433 nm was imaged onto the slits of a 0.46-m monochromator using a 150-mm focal length lens and a prism rotator to rotate the slit image parallel to the laser beam. The plasma observation volume was approximately 8 mm in the direction of the pump laser beam, 0.5 mm high and 4 mm wide. For each data point, fluorescence from 256 laser pulses was integrated using a transient digitizer. The LIF was observed to scale linearly with input energy. In previous work, the LIF imaging system was perpendicular to the pump laser beam. In that geometry, the maximum radial extent that could be observed was r = 6 cm. For this experiment, the LIF detection system was rotated about the center of the discharge chamber approximately 25 degrees to enable observation of LIF at larger radial positions. Vignetting due to the discharge walls and windows was monitored by placing a 1 mm diameter point source (masked mercury spectral calibration lamp) in the center of the LIF observation area and translating the discharge chamber. For these measurements, vignetting was not a significant correction. In all cases, the laser induced fluorescence was well fit by a single exponential decay. The relative density of the $1s_5$ and $1s_4$ levels was determined by the height of the exponential fit normalized to the laser power.

Electron density and temperature (T_e) was measured using a floating double probe system. The probe potential was swept at 100 to 400 Hz and the probe characteristics were fit to theory[25, 26] using a interative optimization scheme.[27] Computed values of T_e were reproducible to less than 0.1 eV. The relationship of the computed T_e to the actual distribution function was uncertain except that the double probe technique tends to sample the higher-energy tail of the energy distribution function.

III. Results and discussion

A. Discharges in argon

The relative density of the $1s_5$ and $1s_4$ levels in the center of the discharge as a function of rf power is shown in Fig. 1 for two pressures. These measurements were obtained 2 cm above the lower electrode and in the center of the discharge, r = 0 cm. The radial distribution for these conditions (10 mTorr) is shown in Fig. 2. As the power was increased, the $1s_5$ density in the center of the discharge decreased approximately 20 percent at 10 mTorr and 50 percent at 40 mTorr. As will be discussed in the next section, the larger decrease with increased rf power for the 40 mTorr case was likely due to enhanced gas heating. The decrease is not likely due to electron driven collisional processes (at least to first order) since both production and loss terms are proportional to electron density. Finally, the observed trends in the $1s_5$ density are consistent with the slightly decreasing line integrated density observed in previous measurements in the system.[5]

The relative density of the $1s_4$ level has some similarities and notable differences with the power dependence of the $1s_5$ level. As the power was increased, the $1s_4$ density in the center of the 40-mTorr discharge also decreased approximately 50 percent. However, for the 10-mTorr

case, the density of the $1s_4$ level increased slightly and then became constant. In addition to the density in the center increasing with rf power, the spatial distribution changed. As the rf power was increased, the $1s_4$ density in the center was approximately constant while the density at the edge increased. The edge increase may be due to enhanced electron collisional driven transfer from the $1s_5$ state at the edge as the power and electron density were increased. The differences in the $1s_4$ and $1s_5$ power dependence are likely due to the contributions of both radiation trapping and electron collisional transfer from the $1s_5$ state to the production / loss balance for the $1s_4$ level.[28, 29] As pressure increases, the importance of radiation trapping in enhancing the $1s_4$ density increases. In addition, increasing the electron density by increasing the pressure or power will increase the density of the $1s_4$ level due to enhanced collisional transfer from the $1s_5$ and $1s_3$ metastable levels. Finally, the spatially resolved measurements are consistent with the previously measured line integrated density.[5] In those experiments, the $1s_4$ line integrated density first increased with rf power and then was constant for powers greater than 150 W.

Increasing the pressure for a constant rf power generally resulted first in an increase in the $1s_5$ and $1s_4$ density and then in a decrease. Figure 3 shows the relative density of the $1s_5$ and $1s_4$ energy levels in the center of the discharge as a function of pressure while the spatial distribution is shown in Fig. 4. For a power of 100 W, the $1s_5$ density increased approximately 50 percent as the pressure was increased from 5 to 25 mTorr and then decreased as the pressure was increased to 50 mTorr. For higher rf powers, the density was approximately constant to decreasing as the pressure was increased above approximately 25 - 30 mTorr. The initial increase is likely related to increasing production of the $1s_5$ state due to the increasing electron density. As the pressure and electron density further increase, the loss processes begin to dominant and the $1s_5$ density decreases. Experimentally, metastable temperature did not strongly

depend on pressure.[5] The location of the broad maximum may be due to the power dependence of the electron density superimposed on the pressure dependence of the electron-density-driven production / loss balance. As shown in the spatial profiles, the decrease of the $1s_5$ density in the center was accompanied by a smaller decrease in the density at the edge of the discharge. Thus increasing the pressure resulted in a general decrease in the $1s_5$ density at all locations of the discharge, but the fractional change was greatest in the center of the plasma. Again this is likely due to electron collisional effects since the electron density was highest in the center of the discharge.[24] The observed trends in the spatially resolved $1s_5$ density are consistent with the previous line integrated measurements that showed a slight increase in line integrated density from 5 to 10 mTorr and then a small decrease in the line integrated density as the pressure was increased from 10 to 50 mTorr.[5]

The density of the $1s_4$ state in the center of the discharge first increased as the pressure was increased from 5 to 20 mTorr and then was constant for higher pressures. For the lowest power of 100 W, the increase was a factor of 4 while the higher powers had smaller relative increases. The initial increase in $1s_4$ density is consistent with electron-collision-enhanced production of the $1s_4$ either directly from the ground state or other 1s level. However, the constant density at higher pressures is in contrast to the decreasing density of the $1s_5$ metastable level and may be related to both enhanced radiation trapping at higher pressures and transfer from the $1s_5$ level. The spatial profiles showed the $1s_4$ density increased at the edges of the discharge while the density in the center was approximately constant; in line with the previous line integrated density measurements that showed a factor of two increase in the line integrated density as the pressure was increased from 10 to 50 mTorr.[24] The increased width of the $1s_4$

spatial distribution may be due to the increased importance of radiation trapping at higher pressures.

The spatial distributions of the $1s_5$ metastable level for several heights above the lower electrode are shown in Fig. 5. Moving away from the induction coil and towards the lower electrode, the density in the center of the discharge, r = 0 cm, decreased while the value at the edge of the discharge, r = 6 cm, was constant. This resulted in a flatter spatial distribution and suggests that the major source of metastables is in the regions next to the rf coils. This argument is supported by the observed decrease in electron temperature with increased distance from the source.[24]

By combining these LIF measurements of the relative spatial metastable density and previous absolute line integrated density measurements along radial cords, information about the absolute spatially resolved density can be derived.[5] In addition, it is possible to derive information about the spatial temperature distribution. In the previous analysis of the line integrated density, the absorption lineshape as a function of radial and axial position was recorded.[5] The lineshapes were then fit to a theoretical Voigt lineshape that assumed a uniform temperature and density. While that assumption was clearly not correct in light of these measurements, it was previously noted that a nonuniform spatial distribution would have the effect of averaging the density while not significantly impacting the temperature due to the different influence of those two parameters on the integrated lineshape.

To simplify the derivation of an absolute density for the spatially resolved $1s_5$ level from the LIF and absorption measurements, we assumed a Gaussian functional form for the radial number density of

$$N_m(r) = N_0 \exp(-4\ln 2\ (r/\Delta r_m)^2) \qquad (1)$$

where N_m is the radially dependent density, N_0 is the peak density and Δr_m is the FWHM of the distribution. An example of the fit for the spatially resolved $1s_5$ energy level in a 10 mTorr, 200 W discharge is shown in Fig. 6a. The measured LIF spatial profile was well fit by a Gaussian with a FWHM of 12 cm. The temperature profile is assumed to have a functional form of

$$T_m(r) = 300 + T_0 \exp(-4\ln 2\ (r/\Delta r_t)^2) \qquad (2)$$

where T_m is the radially dependent temperature, T_0 is the increase in the temperature above room temperature at the center and Δr_t is the FWHM of the distribution. These radial density and temperature profiles were used to generate simulated absorption lineshapes along cords as functions of distance from the center of the discharge. The parameters of peak density, temperature and temperature FWHM where then optimized to give the best fit to the previously measured line integrated density and temperature. The optimization routine was identical to the code used to fit the previous absorption data and used a downhill simplex method with simulated annealing to avoid local minima in the optimization.[27] For the case shown in Fig. 6, the optimization routine returned a peak density of 3.4×10^{11} cm^{-3}, temperature of 300 + 550 = 850 K and a temperature FWHM of 16 cm. The resultant fits to the line integrated data capture most of the features of the previous absorption data with the exception of the relatively constant line-integrated density in the center of the discharge. This may be due to the assumed Gaussian function for the density distribution. While a Gaussian profile appears to be correct in the center of the discharge, the values beyond r = 7 cm to the chamber windows may not be well fit by a Gaussian. An enhanced tail in the density distribution at r > 7 cm would result in the observed departure from the measured and fit line integrated density. The temperature of 850 K is in excellent agreement with the results of separate LIF measurements of the $1s_5$ temperature in the center of the discharge.[4]

By examining the fits for several powers and pressures, and looking at the details of the Voigt line shape function, several points were noted. The peak density is approximately a factor of two higher than the line integrated density assuming a path length of 12 cm. This is exactly what would be expected by averaging the Gaussian density profile. In addition, the temperature in the center of the discharge is in good agreement with both the number determined from separate LIF measurements and the value derived from the lineshape assuming a uniform temperature distribution. An examination of the effect of temperature on the lineshape shows that the characteristics of the lineshape that depend on temperature are influenced by the maximum temperature through which the probe beam propagates, not the average temperature. Thus a fit of the lineshape for these conditions tends to capture the peak temperature. Finally, the spatial temperature distribution is significantly broader than the spatial density distribution. This is likely the result of the different mechanisms that influence the spatial distribution of the density and temperature; electron collisions are important in determining the metastable density while neutral collisions are important for transferring heat. For these discharge conditions, the mean free path of an electron is much shorter than that of a neutral atom.

B. Global model of argon 1s populations

In an attempt to understand better the relative importance of competing processes in the argon discharges, we developed a simple global model (spatially averaged) for creation and destruction of 1s states. The model focused on the distinct behavior of the four closely coupled 1s levels and it did not include a plasma model. The model was a set of four coupled rate equations, one for the density n_i in each level, as follows.

$$\dot{n}_i = \alpha_i n_e N_0 - \beta_i n_e n_i - \chi_i n_e n_i + n_e \sum_{j=1,\neq i}^{4} (a_{ji} n_j - b_{ij} n_i) - \gamma_i n_i \sum_{j=1}^{4} n_j - A_{eff} n_i - D n_i / \Lambda^2 \qquad (3)$$

The terms on the right side represent, respectively,

1. formation by electron collisions with ground-state argon atoms (density N_0),
2. deexcitation to the ground state by superelastic electron collisions,
3. destruction by ionizing collisions with electrons,
4. conversion (mixing) between states $1s_i$ and $1s_j$ due to electron collisions,
5. destruction due to collisions between two atoms in the 1s states,
6. radiative decay with trapping from the $1s_2$ and $1s_4$ states, and
7. loss by axial diffusion to the coupling window and the lower electrode.

The rates for terms 1, 2, 3 and 4 were computed from cross sections assuming Maxwellian distributions of electrons. Terms 1, 2, and 4 used cross sections computed by Bartschat and Zeman[30] along with detailed balance, and term 3 used cross sections from McGuire[31] and Hyman.[32] Term 5 used a single rate (5×10^{-16} m^3/s) for all states.[33] Term 6 employed trapping as described by the Holstein formulation for slab geometry.[28,29,34] The effective A coefficient was the radiative coefficient multiplied by the larger of the escape factors appropriate for Doppler and natural broadening. We also tested the analytic treatment of Lawler and Curry[35] and obtained results that were generally similar but they did not agree quite as well with the measurements. For the high excited-state densities and low pressures of our experiment, neither approach was totally applicable because resonance collisions were not frequent enough to cause frequency redistribution. Diffusive loss, term 7, used an estimated diffusion coefficient (1×10^{-5} m^2/s at STP). Energy levels, degeneracies, and radiative lifetimes were taken from Wiese, Smith, and Miles.[36] The model did not include higher-state populations. For reasonable

impurity levels and cross sections, Penning ionization processes did not appear to be important and were not included in the final model.

Because the model addressed only the excited-state behavior and not the plasma properties, gas temperature, n_e, and T_e were treated as specified functions of the independent variables pressure and power. Figure 7 shows measured values of n_e and T_e (data points) along with empirically derived analytic fits to the data (curves) that were used in the calculations. The neutral gas density was computed from linear fits to the measured pressures and temperatures in Figs. 15 and 16 of Ref. 5.

Figure 8 shows a comparison between line-integrated measurements reported in Ref. 5 and results of the above model. The model predictions agree surprisingly well with the measured 1s densities in absolute value and the model results display most of the observed experimental trends. For example, the $1s_5$ density is always the highest, and, with increasing pressure, the calculated $1s_2$ and $1s_4$ densities approach and exceed the density of the $1s_3$ metastable level. Also, at low pressure, the ordering of the $1s_2$ and $1s_4$ densities changes in both the experiment and the model. The pressures at which the $1s_2$ and $1s_4$ densities equal the $1s_3$ density are about a factor of two higher in the model than in the experiment, which is certainly satisfactory quantitative agreement for this type of model. Such discrepancies are not surprising in light the omission of higher excited levels in the model[37, 38, 39, 40], the uncertainties in cross sections, and the approximate treatment of radiation trapping.

The area of most significant disagreement with the data is the trend in the model for increasing 1s populations with pressure above 20 mTorr. Three possible contributors to this discrepancy have been identified. First, in the parameter range of this work, from 60% to 80% of the total computed destruction rate of the four 1s states, taken as a group, is due to radiative

losses. The remainder of the loss rate is dominated by ionization due to electron impact. Consequently, we suspect that our approximate treatment of radiative losses, which becomes increasingly suspect at higher pressures, is a likely source of the discrepancy. Both of the treatments of radiation transport that we tested (above) displayed the same high-pressure behavior. Note that at the highest pressures in this work, resonance collisional broadening is still unimportant. Second, it is also possible that the error results from a non-Maxwellian electron distribution function whose associated excitation rate decreases more rapidly with pressure than indicated by the Langmuir-probe data. Note that values of T_e from the double probe, which sampled higher-energy electrons, were approximately 1 eV lower than previous measurements[24] from a single probe, which sampled lower-energy electrons. Calculations by Bassett and Economou[41] for dc argon discharges indeed show complex distribution functions, although their work addressed lower n_e values and higher pressures where electron-electron collisions would be less effective at thermalizing the distribution function. If the probe measurements were grossly in error in our work, then the computed absolute densities would probably not agree so well with the data. Third, the global model necessarily ignores changes with pressure that have been measured in the spatial distribution of parameters.

In spite of the limitations of the model, trends in the model allow us to make several observations regarding our present measurements:

1. Diffusion is not a dominant loss process for the 1s states, even at the lowest pressures. Note that diffusion should be affected by the strong axial gradients in neutral-gas temperature and density, which are not addressed in the global model. The rapid increase of $1s_2$ and $1s_4$ density with pressure in the 4 to 20 mTorr range is due to radiation

trapping becoming more effective with increasing gas density, rather than due to a reduction in diffusion losses.

2. The Holstein formulation for radiation transport implies that the measured crossover in $1s_2$ and $1s_4$ populations near 5 mTorr is due to a change in radiation transport from being dominated by Doppler broadening to being dominated by natural broadening. However, this feature in the data was not displayed when the Lawler-Curry transport treatment was used.
3. Mixing and trapping are both necessary for the $1s_2$ and $1s_4$ densities to approach the $1s_3$ and $1s_5$ densities with increasing pressure.
4. The decrease in 1s densities with increasing power at constant pressure (Fig. 1) is due to the reduction in gas density caused by gas heating. This effect is not evident in the previous, line-integrated data in Fig. 8. This discrepancy may be due to variations with power of the spatial distributions of the species (Fig. 2).
5. Destruction of 1s states by electron superelastic collisions (term 2 above) and by mutual collisions among 1s states (term 5 above) do not occur at significant rates compared to other processes in the parameter range of this experiment.

We are encouraged by the relative success of this global model in capturing the major features of the argon measurements. The processes identified in the model would be important elements of a more comprehensive treatment of the discharge physics, which might help to clarify issues surrounding radiation transport such as observation #2 above.

C. Spatially resolved fluorescence lifetimes and quenching

The LIF lifetime was a function of discharge condition. As shown in Fig. 9a, increasing the pressure decreased the LIF lifetime for a constant rf power. These measurements were obtained in the center of the discharge, r = 0 cm and z = 2 cm. For the lowest power of 100 W, the fluorescence lifetime decreased approximately a factor of 3, from 90 to 35 ns as the power was increased. A plot of 1 / lifetime as a function of pressure is shown in Fig. 9b. The lines are best-fit linear regressions. The slope gives the quenching rate and the zero intercept the natural lifetime. The quenching rates were 2.8×10^{-8}, 5.6×10^{-8} and 8.8×10^{-8} cm^3 s^{-1} for rf powers of 100, 200 and 350 W respectively. In calculating the quenching rate, the pressure in the center of the discharge was deduced using the ideal gas law and the measured temperatures of 600, 800 and 1000 K for rf powers of 100, 200 and 350 W, respectively.[5] The zero intercept gives lifetimes of 127, 104 and 67 ns for rf power of 100, 200 and 350 W, respectively.

The impact of electron collisional quenching is clearly observed in these measurements. As shown in Fig. 9c, the quenching rates were a linear function of plasma power, as was the electron density.[24] For this plot, the quenching rates were plotted as a function of power into the plasma since previous measurements of the electron density showed that the electron density was a linear function of the plasma power with a zero intercept.[24] Inoue et. al examined the radiative lifetime and collisional quenching rates for the $3p_3$-to-$1s_2$ transition in the afterglow of an argon discharge specifically to avoid the influence of electron collisions.[42] For the $3p_3$-to-$1s_2$ transition, they measured a lifetime of 123 ± 11 ns transition and a quenching rate constant of 4.2×10^{-10} cm^3 s^{-1}. Within the uncertainties, the quenching rates and lifetimes derived by extrapolating our measurements to zero power are consistent with the measurements of Inoue et al.

The lifetime was also a function of power and radial position. Figure 10 shows the fluorescence lifetime as a function of rf power while Fig. 11 shows the fluorescence lifetime as a function of radial position for several discharge conditions. The lifetimes were smallest for the highest powers and in the center of the discharge, where the electron density was maximum.[24] At larger radial position, the lifetime increased, with a possible asymptote at approximately 130 - 140 ns, in line with the measured lifetime of 123 $\pm$ 11 ns.[42]

D. Influence of chlorine or boron trichloride addition

In some applications, argon is added to the gas mixture in order to stabilize the discharge or dilute the active gases while maintaining a constant chamber pressure. Previous work has examined the influence of argon addition on a number of plasma species such as electron, Cl^-, metastable Cl^+, Cl and BCl density.[16,18,19,20,21,22] By combining previous measurements of the molecular dissociation products and the negative ions with our measurements of the argon excited state distributions, the influence of argon excited states on Cl_2 and BCl_3 dissociation can be investigated. Fluorescence lifetime data is also significant since the effects of excited state quenching were found to be gas mixture dependent.

The relative density of the $1s_5$ metastable level, $3p_3$-to-$1s_2$ fluorescence lifetime, and electron temperature are shown in Fig. 12 as functions of Ar / Cl_2 or Ar / BCl_3 ratio. As Cl_2 or BCl_3 replaced the argon, the metastable density first increased and then decreased. The increase was significantly greater in Cl_2 than BCl_3. Over this same parameter space, the fluorescence lifetime increased from 40 to 70 ns, likely due to changes in the argon density or electron density.[22] For argon fractions less than 40 percent, the electron temperature was relatively constant. Thus changes in the 1s state density can be attributed to changes in only the electron

and neutral density. The increase in electron temperature for mostly Cl_2 mixtures (Fig. 12c) is not understood but may be related to a shift in the dominant positive ion. The magnitude and shape of the temperature jump was quite stable and reproducible, and we were unable to identify any probe artifact that contributed to the observation.

The scaling for the $1s_5$ density with molecular gas addition in the inductively coupled discharge had both similarities and differences with previous measurements in parallel plate and ECR discharge systems. For example, Scheller et al observed first an increase and then a decrease in the $1s_5$ density as SF_6, Cl_2 and BCl_3 were added to an argon parallel plate rf discharge.[8] However, they observed that the peak in argon metastable density occurred at an added gas mole fraction of less than 0.01, considerably less than the observed peak in our measurements. Leonhardt et al reported that the $1s_4$ density peaked for a chlorine fraction of approximately 15 percent in a 1-mTorr ECR discharge.[9] Scheller et al and Leonhardt et al have argued that the increase in argon metastable density was likely due to a decrease in electron density due to formation of negative ions by dissociative attachment. The decrease in density of low energy electrons would reduce the loss rate of the metastable by mixing, resulting in an increase in the metastable density. However, at some dilution, the electron density would become too small and the production of the argon metastable by electron impact begins to fall.

Comparison of our current results with our previous measurements of the electron and negative ion density for these discharge conditions strongly supports this hypothesis. As the argon fraction was reduced from 1 to 0.7, we have measured in Cl_2 an almost factor of two decrease in the electron density and an enhanced negative ion density.[22] The difference between the ratio at the peak of the metastable density in Cl_2 and BCl_3 containing mixtures is likely related to the different cross sections for negative ion formation. Previous work has shown that

the negative ion density in a Cl_2 discharge was a factor of four higher than a BCl_3 discharge but the electron density was the same.[22] In our previous measurements of the negative ion and electron density in Ar / Cl_2 mixtures, we reported an unexpectedly high Cl^- density at low Cl_2 fractions in argon.[22] Based upon the recent electron temperature measurements, we can attribute the enhanced Cl^- density at low Cl_2 fraction to a high electron density and a low electron temperature.

The electron loss mechanism argument discussed above can be extended to explain some of the differences observed between the ICP, ECR, and parallel plate discharges. The occurrence of the peak in argon metastable density at higher chlorine fractions in the ICP system than in the parallel plate system is likely due to a higher electron density in the ICP. The higher electron density in the ICP would result in more electrons being available for negative ion formation without significantly reducing the fraction used to produce the metastable state. These two processes use different parts of the electron energy distribution since negative ion formation favors low energy electrons while the high energy tail is required to sustain the discharge and produce a metastable state by direct ionization (11.5 eV). In addition, the parallel plate discharge operated at a significantly higher pressure than the ICP, which would enhance negative ion formation and electron loss.[8] All of these mechanism would lead to a faster decrease in the metastable density with molecular gas addition in the parallel plate system compared with the ICP system. The interpretation of the ECR results likely follows a similar argument but is clouded by the contribution of radiation trapping to the production / loss balance of the measured $1s_4$ level.[9]

The change in argon metastable density with pressure is shown in Fig. 13 for two gas mixtures. As the pressure was increased, the argon metastable density decreased in the BCl_3 / Ar

mixture but not the Cl_2 / Ar gas mixture. The decrease in the BCl_3 containing gas mixture may be due to enhanced quenching of the metastable density by either BCl_3 or one of its decomposition products, or a change in the electron density. Unfortunately, no electron density data in Ar / BCl_3 mixtures was available to check the hypothesis. The suggestion of different quenching rates for BCl_3 and Cl_2 is weakly supported by the difference in the excited state fluorescence; the fluorescence lifetime in BCl_3 / Ar mixtures tends to increase with pressure while the Cl_2 / Ar mixtures tend to decrease.

As shown in Fig. 14, increasing the rf power in mixtures of argon and Cl_2 or BCl_3 resulted in an increase in the argon metastable density. The increase was slightly larger in the gas mixture containing BCl_3. The increase in metastable density is in contrast to the monotonic decrease in $1s_5$ density as the power was increased in a pure argon discharge (Fig. 1). Previous measurements in Ar / Cl_2 mixtures showed that the electron density increased linearly with rf power while the negative ion density was constant.[22] If the low energy electrons are removed from the discharge by negative ion formation while the total electron density goes up, then the metastable production by impact of an electron with ground state would increase while the loss of the $1s_5$ metastable by low energy electron mixing will decrease. The net result would be the observed increase in $1s_5$ density with power. For both gas mixtures, the lifetimes decreased with increased rf power. The decrease was similar to that observed in pure argon discharges but the lifetimes in pure argon were smaller, indicating more quenching of the upper state in pure argon than in argon containing mixtures.

The radial profile of the metastable density in pure argon and Ar / Cl_2 gas mixtures is shown in Fig. 15. As Cl_2 replaced argon, the density in the center changed, but the FWHM of the spatial distribution was approximately the same. Thus adding Cl_2 to the argon plasma

appeared to have little effect on the spatial distribution, only on the absolute density. However, the fluorescence lifetime increased with chlorine addition, consistent with the measurements in the center of the discharge. As with the pure argon discharge, the increase in the lifetime at the edge of the plasma is likely due to reduced electron collisional effects since the spatial distribution of electrons in Ar / Cl_2 gas mixtures is similar to the pure argon discharge.[20,24]

The relative $1s_5$ metastable density when argon is added to a gas mixture containing Cl_2 / BCl_3 is shown in Fig. 16. For this experiment, argon was added and the total pressure was kept constant as the total flow rate increased. A linear increase in the argon flow rate resulted in a linear increase in the $1s_5$ metastable level. The linear increase in the argon metastable density is consistent with previous measurements that showed no change in the electron, Cl^-, Cl_m^+ or BCl density as argon was added to the plasma.[16,18,19,20,21,22] Thus argon excited state collisions appear to have little direct influence on the molecular dissociation of Cl_2 or BCl_3. In addition, the fluorescence lifetime was constant. This is in contrast to the decreased fluorescence lifetime observed in pure argon as the pressure was increased and is likely due to the constant electron density.

IV. Summary

Laser induced fluorescence has been used to measure the spatial distribution of the two lowest energy argon excited states, $1s_5$ and $1s_4$, in inductively driven plasmas containing argon, chlorine and boron trichloride. As demonstrated by our simple global model, electron driven collisional transfer processes such as mixing and ionization play a major role in determining the density of the excited states. In addition, radiation trapping plays an important role in determining the $1s_4$ state density, and indirectly the $1s_5$ metastable density via mixing. Under

some plasma conditions, the $1s_4$ and $1s_5$ densities were comparable. Electron temperature changes may play a very minor role in the mixing processes since the temperature does not vary greatly.

Measurements in pure argon of the spatially resolved excited state density were combined with previous measurements of the line-integrated density to derive absolute spatially resolved excited state distributions. The peak density is approximately a factor of two higher than the line integrated density assuming a path length of 12 cm. In addition, the temperature in the center of the discharge is in good agreement with both the values determined from separate LIF measurements and the value derived from the lineshape assuming a uniform temperature distribution. The spatial temperature distribution is significantly broader than the spatial density distribution. This is likely the result of the different mechanisms that influence the spatial distribution of the density and temperature; electron collisions are important in determining the metastable density while neutral collisions are important for transferring heat.

Cl_2 and BCl_3 were added to the argon discharge to examine the influence of argon excited states on molecular dissociation. Comparison of these measurements with previous measurements of the atomic chlorine and BCl density shows no changes in the Cl or BCl density that can be clearly attributed to direct metastable dissociation of the molecular species. While it is energetically possible for the $1s_5$, $1s_4$, $1s_3$ and $1s_2$ levels to dissociate some of the molecular species present in this discharge, it does not appear to be a significant source of dissociation. The major source of interaction between the argon and the molecular species BCl_3 and Cl_2 appears to be through modification of the electron density and possibly the electron energy distribution function. We noted an interaction between the argon and the Cl^- density in Ar / Cl_2

gas mixtures. However, this interaction can be attributed to changes in the electron density, not to changes in the molecular dissociation.

V. Acknowledgments

The authors thank C. B. Fleddermann, W. J. Alford, and M. E. Riley for many helpful discussions. The authors appreciate the assistance of Professor Klaus Bartschat in obtaining and using the results of his cross-section calculations and helpful discussions with Professor James Lawler concerning approaches to modeling transport of trapped radiation. The technical assistance of T. W. Hamilton is gratefully recognized. This work was performed at Sandia National Laboratories and supported by the United States Department of Energy (DE-AC04-94AL85000).

Figure captions

Fig. 1. Relative $1s_5$ and $1s_4$ excited state density in the center of the discharge as functions of power. Argon pressure was of 10 mTorr(●) and 40 mTorr(■), and height above the lower electrode was 2 cm.

Fig. 2. Relative $1s_5$ and $1s_4$ excited state density as functions of radial position for powers of 100 W (●), 200 W (■) and 350 W (▲). The pressure was 10 mTorr and the height above the lower electrode was 2 cm. The multiple points at r = 0 are repeats and provide and indication of the degree of reproducibility.

Fig. 3. Relative $1s_5$ and $1s_4$ excited state density in the center of the discharge as functions of pressure. Power was 100 W (●), 200 W (■) and 350 W (▲), and height above the lower electrode was 2 cm.

Fig. 4. Relative $1s_5$ and $1s_4$ excited state density as functions of radial position for pressures of 10 mTorr (●) and 40 mTorr(■). The rf power was 200 W and the and height above the lower electrode was 2 cm. The multiple points at r = 0 are repeats and provide and indication of the degree of reproducibility.

Fig. 5. Relative $1s_5$ metastable density as a function of radial position for heights of 3 (●), 2 (■) and 1 (▲) cm above the lower electrode. The pressure was 10 mTorr and the rf power was 200 W.

Fig. 6. Relative $1s_5$ metastable density (a), line integrated density (b) and temperature (c) as functions of radial position for a power of 200 W and a pressure of 10 mTorr. The solid lines are fits to the data discussed in detail in the text.

Fig. 7. Electron density and temperature measured by double Langmuir probe at a location in the middle of the discharge. The global-model calculations used an empirically derived algebraic expression (curves) to approximate the data (points from Ref. 5).

Fig. 8. Comparison of experimental measurements and model predictions. The computed volumetric densities in the model have been converted to areal densities assuming a 10-cm path length.

Fig. 9. Fluorescence lifetime (a) and decay constant (b) in the center of the discharge as functions of pressure. Power was 100 W (●), 200 W (■) and 350 W (▲), and height above the lower electrode was 2 cm. The lines are best-fit linear regressions to each power. (c) shows the quenching rate(◆) and zero intercept lifetime (●) as a function of plasma power.

Fig. 10. Fluorescence lifetime in the center of the discharge as a function of power. Pressure was 10 mTorr (●) and 40 mTorr (■), and height above the lower electrode was 2 cm.

Fig. 11. Fluorescence lifetime as a function of radial position. In figure (a) the pressure was 10 mTorr and in figure (b) the power was 200 W. Height above the lower electrode was 2 cm.

Fig. 12. Relative $1s_5$ metastable density (a), fluorescence lifetime (b), and electron temperature (c) as functions of BCl_3 or Cl_2 fraction in BCl_3 / Ar (●) and Cl_2 / Ar (■) gas mixtures. The power was 300 W, pressure was 20 mTorr and the total flow rate was 10 sccm.

Fig. 13. Relative $1s_5$ metastable density (a), fluorescence lifetime (b), and electron temperature (c) as functions of pressure for BCl_3 / Ar (●) and Cl_2 / Ar (■) gas mixtures. The power was 300 W, and the BCl_3 or Cl_2 flow rate was 5 sccm and the argon flow rate was 5 sccm.

Fig. 14. Relative $1s_5$ metastable density (a), fluorescence lifetime (b), and electron temperature (c) as functions of power for BCl_3 / Ar (●) and Cl_2 / Ar (■) gas mixtures. The pressure was 20 mTorr and the BCl_3 or Cl_2 flow rate was 5 sccm and the argon flow rate was 5 sccm.

Fig. 15. Relative $1s_5$ metastable density (a) and fluorescence lifetime (b) as functions of radial position in two Cl_2 / Ar gas mixtures and pure argon. The pressure was 20 mTorr, the power was 300 W and the total flow rate was 10 sccm. The Cl_2 / Ar flow rates were 0 / 10 (●), 2 / 8 (■), and 5 / 5 (▲).

Fig. 16 Relative $1s_5$ metastable density (a) and fluorescence lifetime (b) as functions of added argon to a BCl_3 / Cl_2 gas mixture. The pressure was 20 mTorr, the power was 300 W, the BCl_3 flow rate was 2.5 sccm and the Cl_2 flow rate was 7.5 sccm. The line is a best-fit linear regression that passes through zero.

[1] F. Ren, J. R. Lothian, J. M. Kuo, W. S. Hobson, J. Lopata, J. A. Caballero, S. J. Pearton and M. W. Cole, J. Vac. Sci. Technol. B **14**, 1758 (1996).

[2] R. J. Shul, G. B. McClellan, R. D. Briggs, D. J. Rieger, S. J. Pearton, C. R. Abernathy, J. W. Lee, C. Constantine and C. Barratt, J. Vac. Sci. Technol A **15**, 633 (1997).

[3] R. J. Shul, R. D. Briggs, S. J. Pearton, C. B. Vartuli, C. R. Abernathy, J. W. Lee, C. Constantine and C. Barratt, Proc. Mat. Resch. Soc. **449**, 696 (1997).

[4] M. V. Malyshev, V. M. Donnelly and S. Samukawa, J. Appl. Phys. **84**(3), 1222 (1998).

[5] G. A. Hebner, J. Appl. Phys. **80**(5), 2624, 1996.

[6] P. A. Miller, G. A. Hebner, R. Jerecki, T. Ni, J. Vac. Sci. Technol. A **16**, 3240 (1998).

[7] B. K. McMillin, M. R. Zachariah, J. Appl. Phys., **79**(1), 77 (1996).

[8] G. R. Scheller, R. A. Gottscho, T. Intrator and D. B. Graves, J. Appl. Phys., **64**(9), 4384 (1988).

[9] D. Leonhardt, C. R. Eddy, V. A. Shamamian, R. F. Fernsler and J. E. Butler, J. Appl. Phys., **83**(6), 2971 (1998).

[10] E. A. Andreev and A. E. Bodrov, Chem. Phys. Lett. **109**, 450 (1984).

[11] K. Tachibana, Phys. Rev. A **34**, 1007 (1986).

[12] J. Johannes, T. Bartel, G. A. Hebner, J. Woodworth, D. J. Economou, J. Electrochem. Soc., **144**(7), 2448 (1997).

[13] E. Meeks, P. Ho, R. Buss, Proc. Electrochem. Soc. (1997), 97-9(Process Control, Diagnostics, and Modeling in Semiconductor Manufacturing), 283-290.

[14] Shahid Rauf, Mark J. Kushner, J. Appl. Phys., **82**(6), 2805 (1997).

[15] D. P. Lymberopoulos, R. S. Wise, D. J. Economou, T. J. Bartel, IEEE Trans. Plasma Sci., **24**(1), 129 (1996).

[16] G. A. Hebner, J. Appl. Phys. **80**(6), 3215, 1996.

[17] G. A. Hebner, J. Appl. Phys. **81**(2), 578, 1997.

[18] G. A. Hebner and C. B. Fleddermann, J. Appl. Phys., **83**, 5102 (1998).

[19] C. B. Fleddermann and G. A. Hebner, J. Appl. Phys, **83**(8), 4030 (1998).

[20] G. A. Hebner, C. B. Fleddermann and P. A. Miller, J. Vac. Sci. Technol A **15**, 2698 (1997).

[21] G. A. Hebner, J. Vac. Sci. Technol. A. **14**(4), 2158 (1996).

[22] C. B. Fleddermann and G. A. Hebner, J. Vac. Sci. Technol. A **15**(4), 1955 (1997).

[23] P. J. Hargis Jr., K. E. Greenberg, P. A. Miller, J. B. Gerardo, J. R. Torczynski, M. E. Riley, G. A. Hebner, J. R. Roberts, J. K. Olthoff, J. R. Whetstone, R. J. Van Brunt, M. A. Sobolewski, H. M. Anderson, M. P. Splichal, J. L. Mock, P. Bletzinger, A. Garscadden, R. A. Gottscho, G. Selwyn, M. Dalvie, J. E. Heidenreich, J. W. Butterbaugh, M. L. Brake, M. L. Passow, J. Pender, A. Lujan, M. E. Elta, D. B. Graves, H. H. Sawin, M. J. Kushner, J. T. Verdeyen, R. Horwath and T. R. Turner, Rev. Sci. Inst. **65**, 140 (1994).

[24] P. A. Miller, G. A. Hebner, K. E. Greenberg, P. D. Pochan and B. P. Aragon, J. Resch. Natl. Int. Standard. Technol **100**, 427 (1995).

[25] F. F. Chen in *Plasma Diagnostic Techniques*, ed by R. H. Huddlestone and S. L. Leonard, Academic Press, New York, 1965, p.p. 113-200.

[26] C. Steinbruchel, J. Vac. Sci. Technol., A **8**, 1663 (1990).

[27] W. H. Press and S. A Teukolsky, Computers in Phys. **5**, 426 (1991).

[28] T. Holstein, Phys. Rev. **72**, 1212 (1947).

[29] T. Holstein, Phys. Rev. **83**, 1159 (1951).

[30] K. Bartschat and V. Zeman, Phys. Rev. **A59** (1999) R2552.

[31] E. J. McGuire, Phys. Rev. **A20**, 445 (1979).

[32] H. A. Hyman, Phys. Rev. **A20**, 855 (1979).

[33] P. K. Leichner and R. J. Ericson, Phys. Rev. **A9**, 251 (1974).

[34] M. E. Riley and W. J. Alford, Sandia Report SAND95-1201 (1995).

[35] J. E. Lawler and J. J. Curry, J. Phys. D: Appl. Phys. **31**, 3235 (1998). To extend the treatment to slab geometry, we used $(2.405/\pi) * \textit{height}$ in place of the radius, by analogy with diffusion.

[36] W. L. Wiese, M. W. Smith, and B. M. Miles, "Atomic Transition Probabilities", National Bureau of Standards publication NSRDS-NBS 22 (1969).

[37] C. M. Ferreira, J. Loureiro, and A. Ricard, J. Appl. Phys. **57**, 82 (1985).

[38] E. V. Karoulina and Yu. A. Lebedev, J. Phys. D: Appl. Phys. **25**, 401 (1992).

[39] A. Bogaerts, R. Gijbels, and J. Vlcek, J. Appl. Phys. **84**, 121 (1998).

[40] U. M. Kelkar, M. H. Gordon, L. A. Roe, and Y. Li, J. Vac. Sci. Technol. **A17**, 125 (1999).

[41] N. L. Bassett and D.J. Economou, J. Appl. Phys. **75**, 1931 (1994).

[42] G. Inoue, D. W. Setser and N. Sadeghi, J. Chem. Phys., **76**(2), 977 (1982).

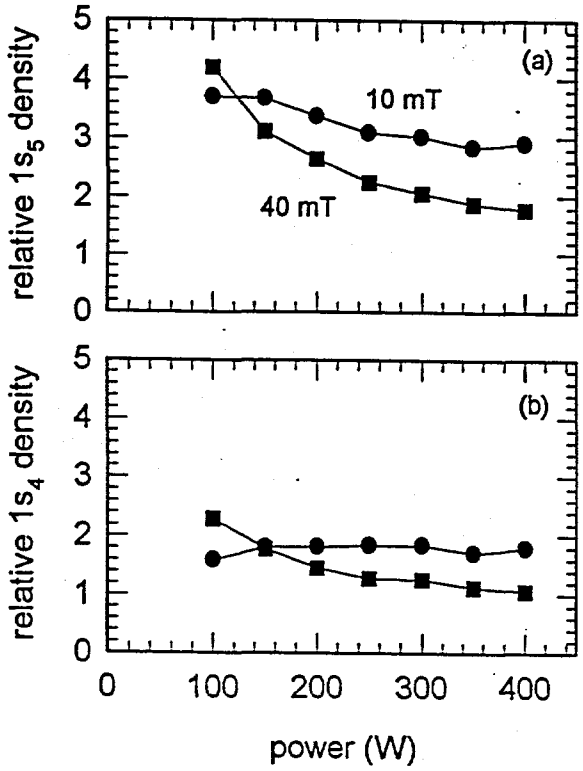
relative $1s_5$ density
(a)
10 mT
40 mT
relative $1s_4$ density
(b)
0
1
2
3
4
5
0
100
200
300
400
power (W)

Fig. 1
Hebner

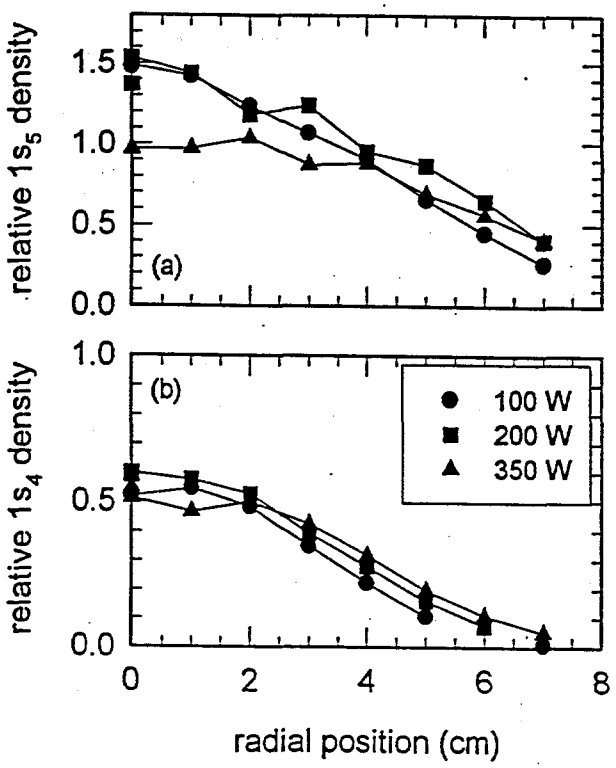
relative 1s5 density
1.5
1.0
0.5
0.0
(a)
relative 1s4 density
1.0
0.5
0.0
(b)
100 W
200 W
350 W
0
2
4
6
8
radial position (cm)

Fig. 2
Hebner

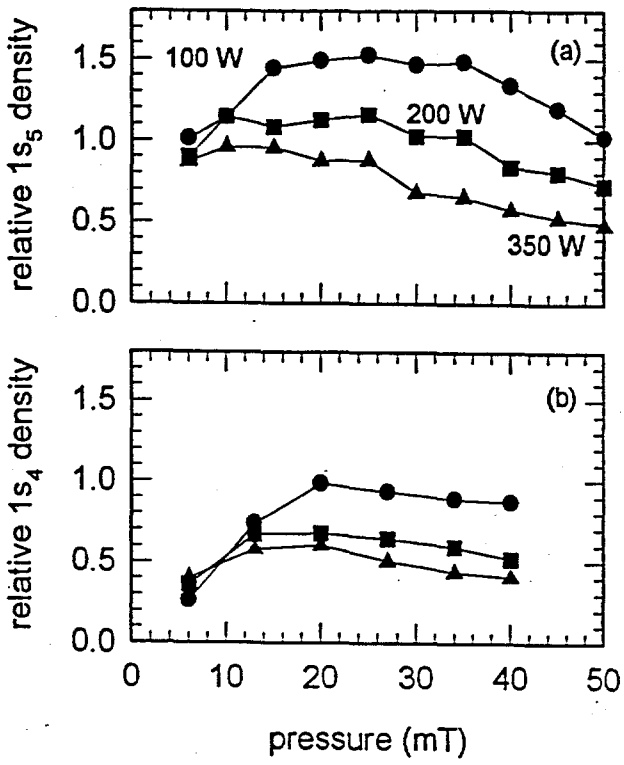
relative 1s5 density
1.5
1.0
0.5
0.0
100 W
200 W
350 W
(a)
relative 1s4 density
1.5
1.0
0.5
0.0
(b)
0
10
20
30
40
50
pressure (mT)

Fig. 3
Hebner

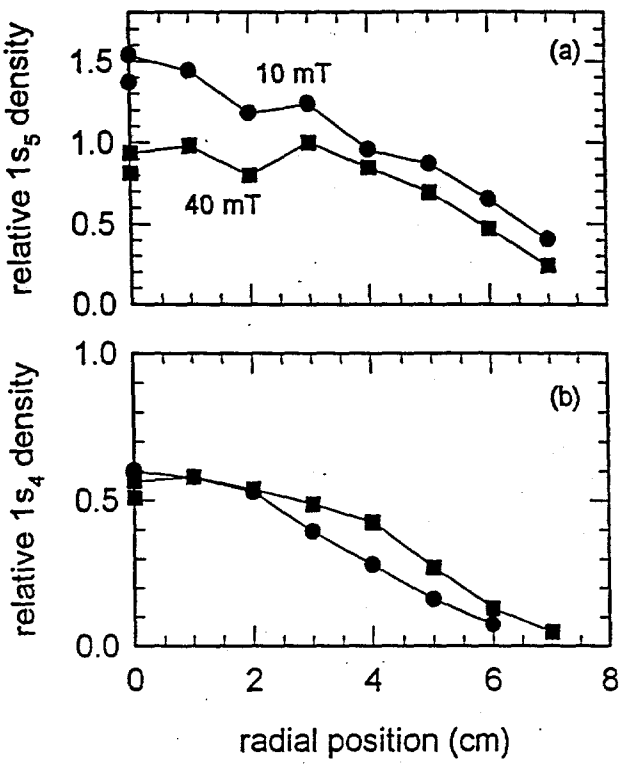
relative 1s5 density
1.5
1.0
0.5
0.0
10 mT
40 mT
(a)
relative 1s4 density
1.0
0.5
0.0
(b)
0
2
4
6
8
radial position (cm)

Fig. 4
Hebner

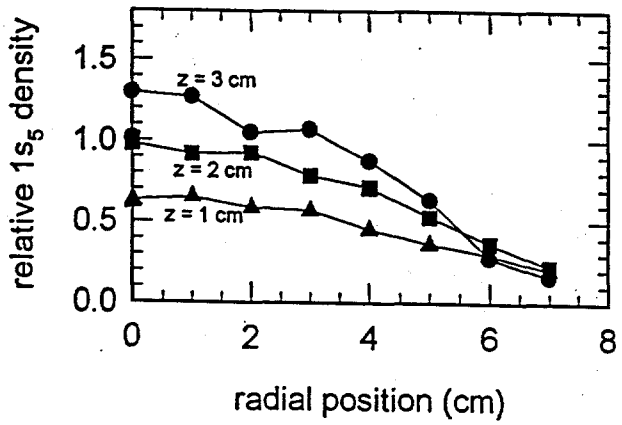
relative 1s5 density
1.5
1.0
0.5
0.0
z = 3 cm
z = 2 cm
z = 1 cm
0
2
4
6
8
radial position (cm)

Fig. 5
Hebner

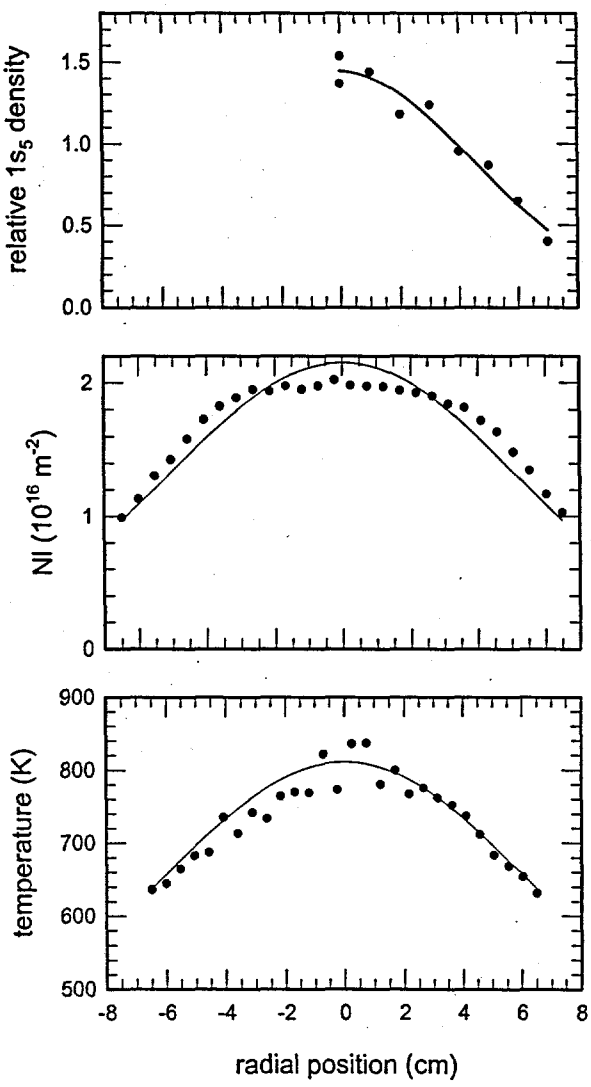
relative 1s5 density
1.5
1.0
0.5
0.0
NI (10^16 m^-2)
2
1
0
temperature (K)
900
800
700
600
500
-8
-6
-4
-2
0
2
4
6
8
radial position (cm)

Fig. 6
Hebner

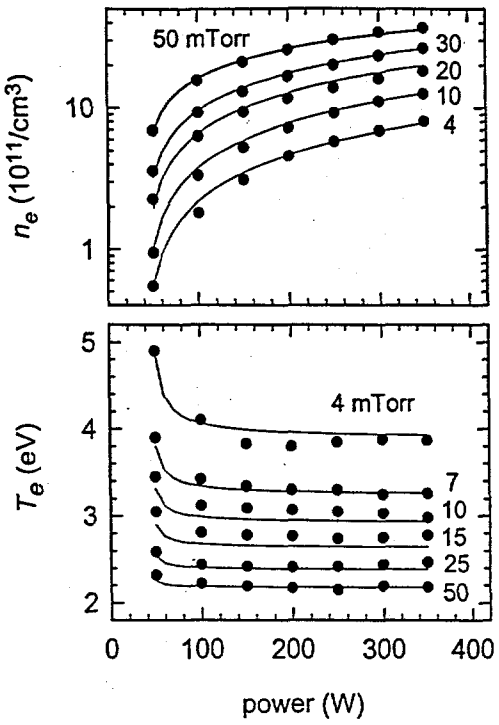
50 mTorr
30
20
10
4
n_e (10^{11}/cm^3)
10
1
4 mTorr
7
10
15
25
50
T_e (eV)
5
4
3
2
0
100
200
300
400
power (W)

Fig. 7
Hebner

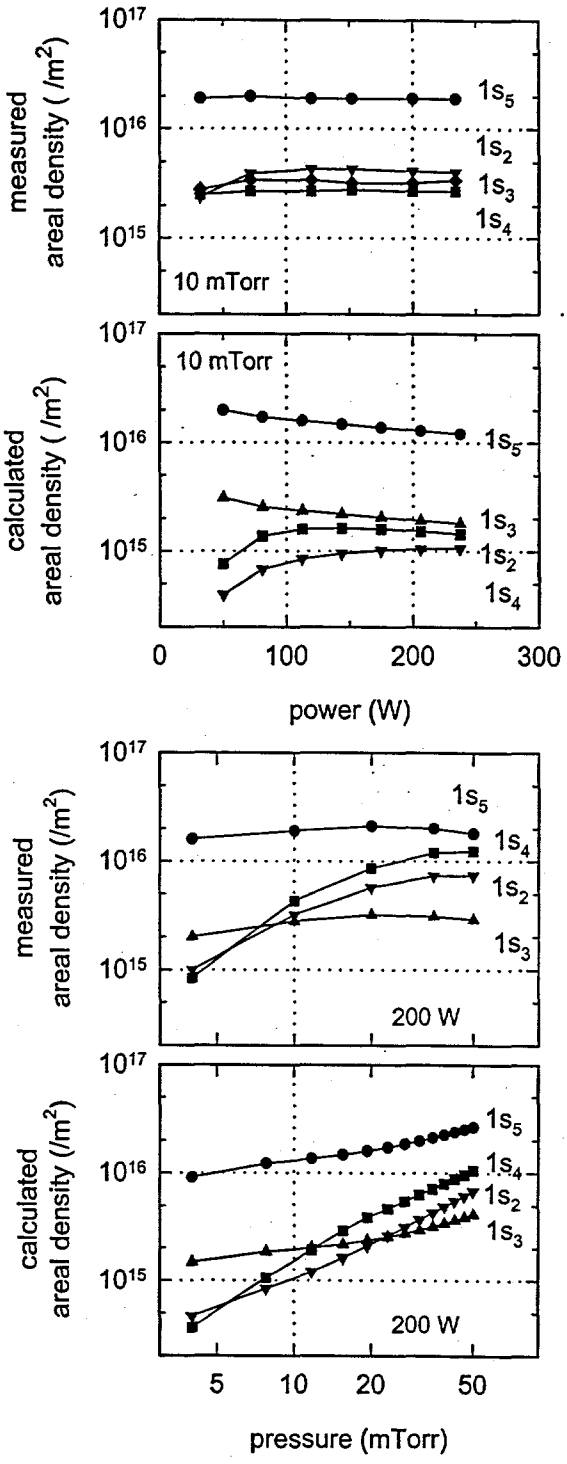
measured areal density (/m^2)
calculated areal density (/m^2)
10^{17}
10^{16}
10^{15}
$1s_5$
$1s_2$
$1s_3$
$1s_4$
10 mTorr
0
100
200
300
power (W)
measured areal density (/m^2)
calculated areal density (/m^2)
200 W
5
10
20
50
pressure (mTorr)

Fig. 8
Hebner

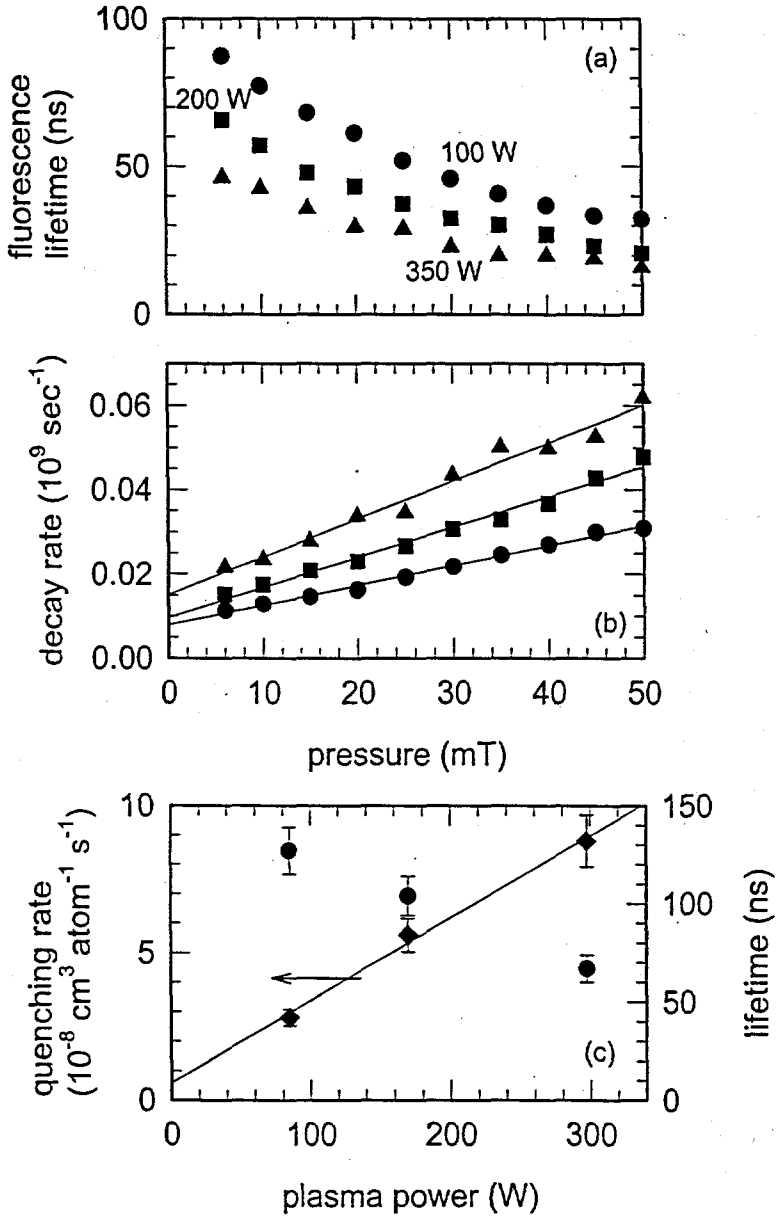
100
50
0
fluorescence lifetime (ns)
(a)
200 W
100 W
350 W
0.06
0.04
0.02
0.00
decay rate (10^9 sec^{-1})
(b)
0
10
20
30
40
50
pressure (mT)
10
5
0
quenching rate (10^{-8} cm^3 atom^{-1} s^{-1})
150
100
50
0
lifetime (ns)
(c)
0
100
200
300
plasma power (W)

Fig. 9
Hebner

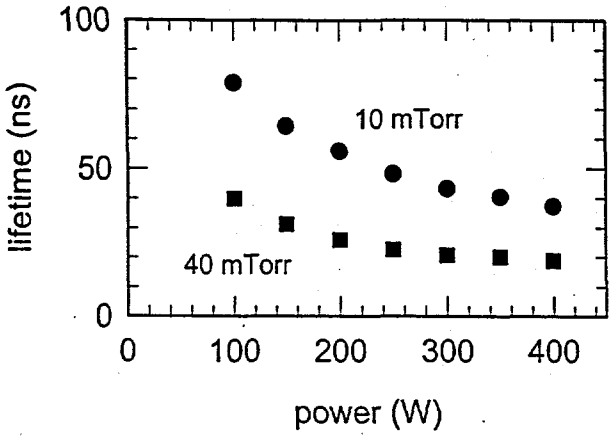

Fig. 10
Hebner

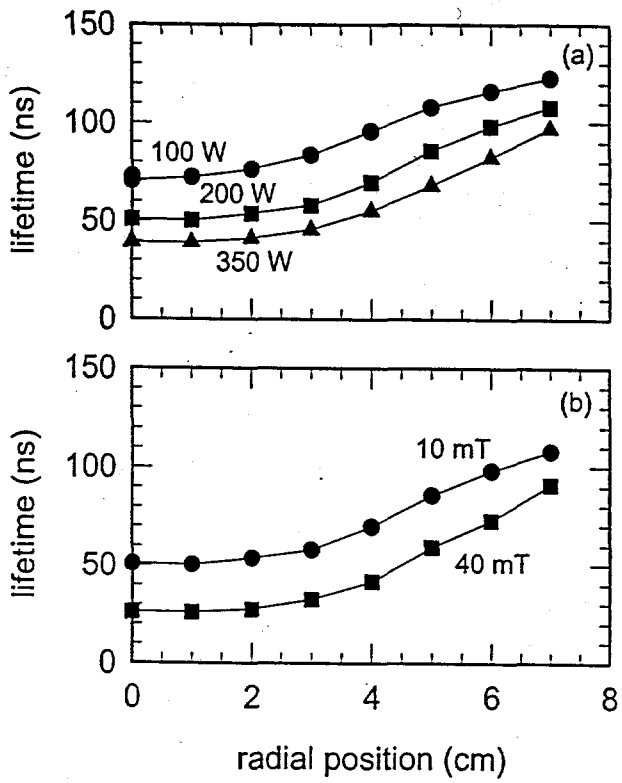

Fig. 11
Hebner

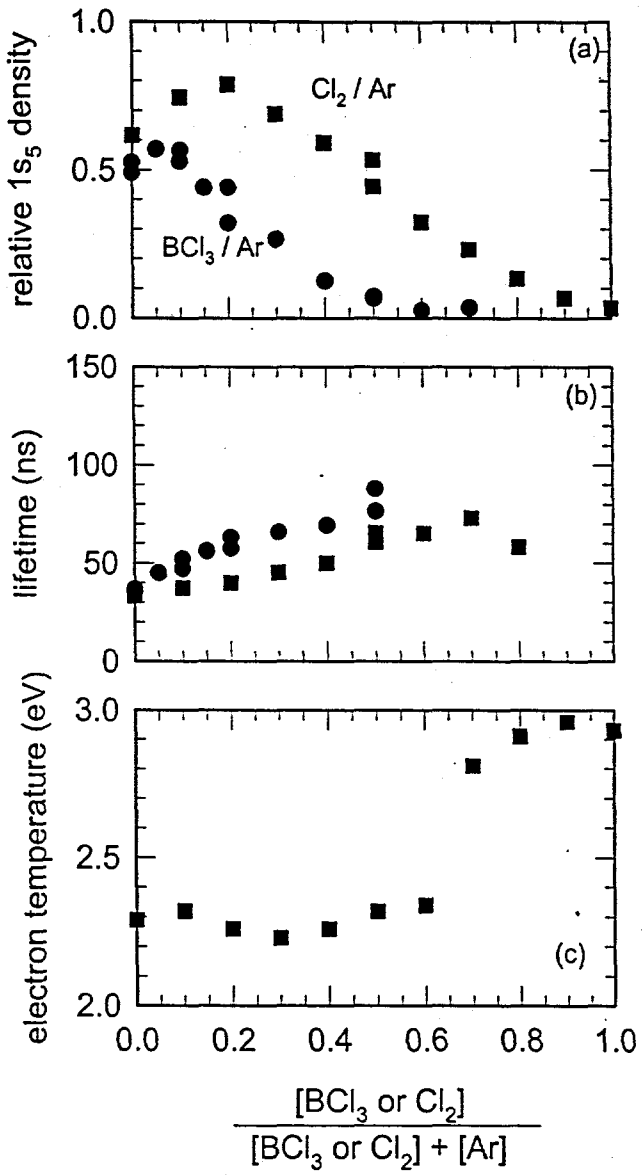

Fig. 12
Hebner

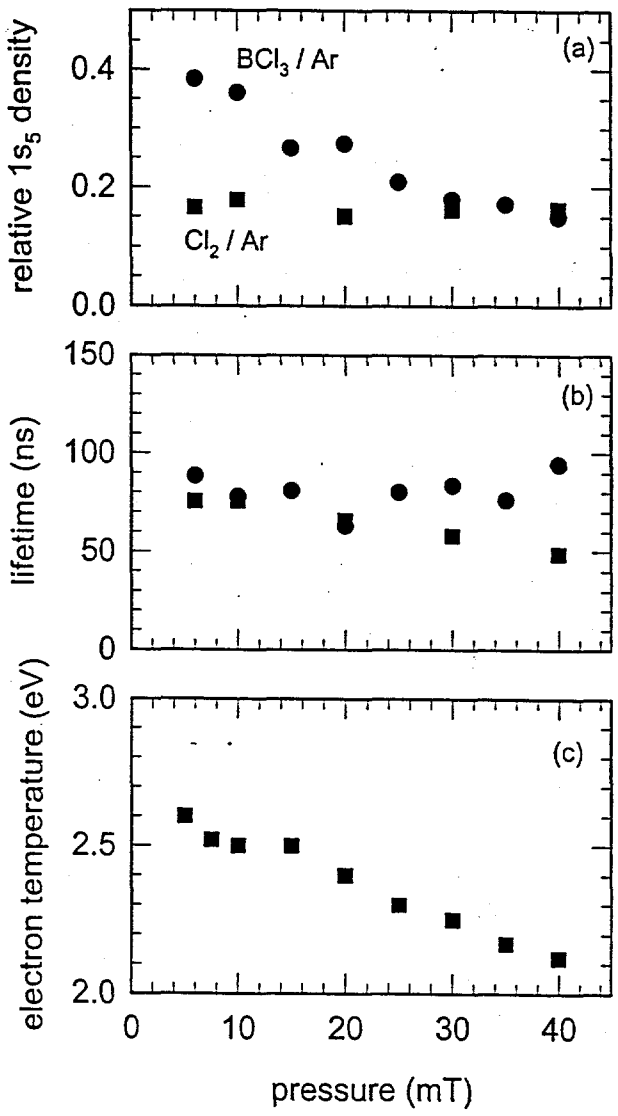

Fig. 13
Hebner

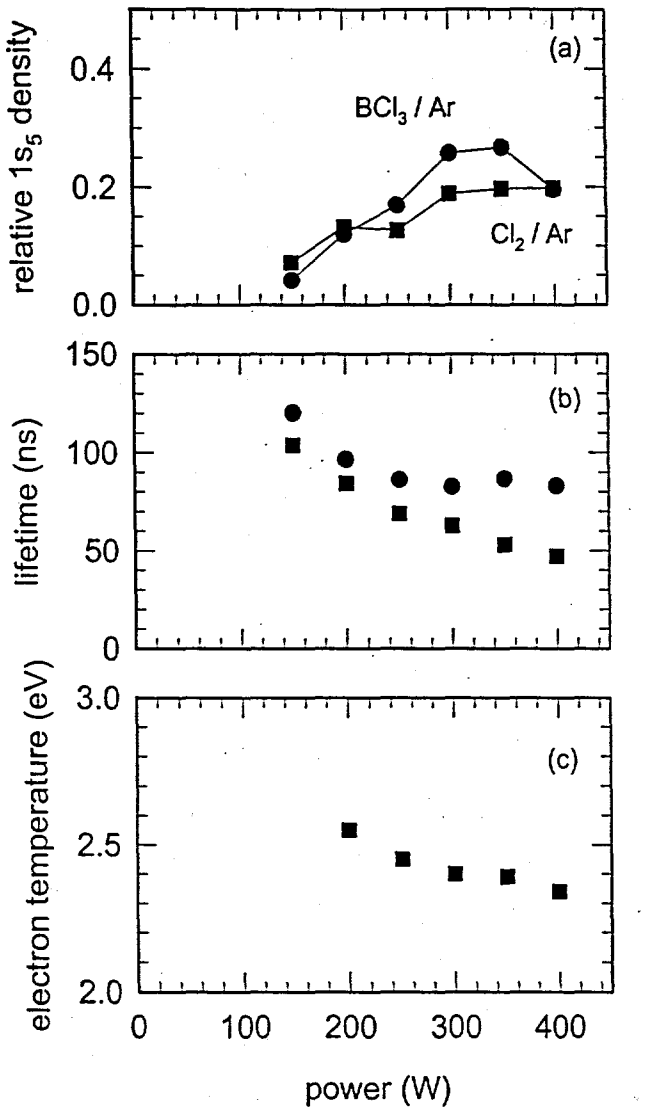

Fig. 14
Hebner

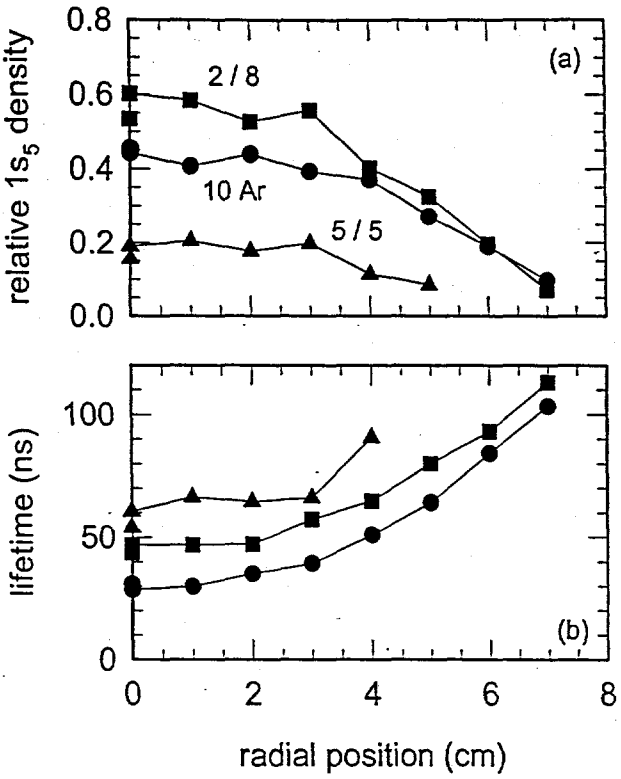

Fig. 15
Hebner

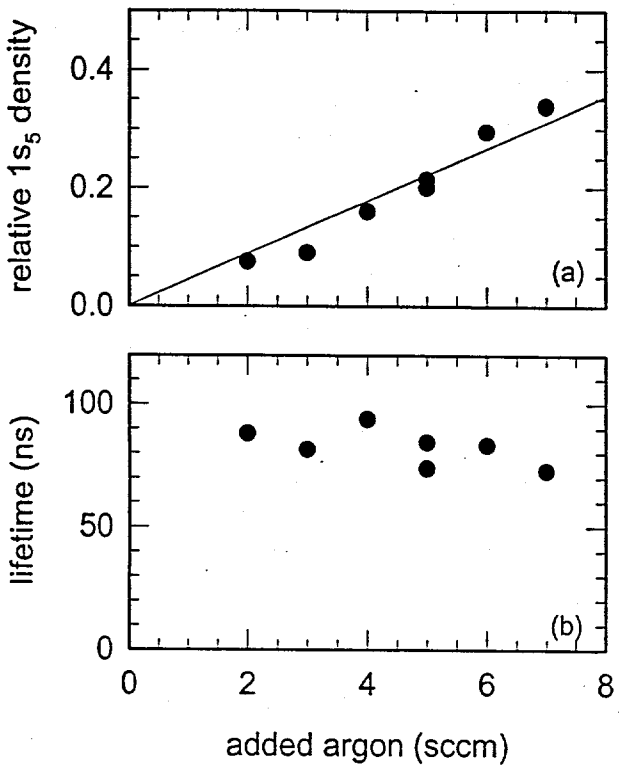

Fig. 16
Hebner